Journal of CO_2 Utilization 19 (2017) 100–111

Contents lists available at ScienceDirect

Journal of CO_2 Utilization

journal homepage: www.elsevier.com/locate/jcou

Optimal Faujasite structures for post combustion CO_2 capture and separation in different swing adsorption processes

Hèctor Prats, Daniel Bahamon, Gerard Alonso, Xavier Giménez, Pablo Gamallo*, Ramón Sayós

Departament de Ciència de Materials i Química Física & Institut de Química Teòrica i Computacional (IQTCUB), Universitat de Barcelona, C. Martí i Franquès 1, 08028 Barcelona, Spain

ARTICLE INFO

Article history:
Received 24 September 2016
Received in revised form 22 February 2017
Accepted 15 March 2017
Available online xxx

Keywords:
Zeolite
CO_2 capture
Sequestration
Molecular simulation
Swing adsorption process

ABSTRACT

Grand Canonical Monte–Carlo (GCMC) simulations are used in this work, to assess optimum faujasite structures, the well–known family of zeolites, in CO_2 capture processes. Pressure Swing Adsorption (PSA) and Vacuum Swing Adsorption (VSA) procedures have been considered to evaluate purity, working capacity and breakthrough time. To this purpose, ten faujasite structures with different Al content were selected, and the best conditions for CO_2 capture maximization have been calculated for each structure. Further results show that zeolites having intermediate Al content are the most effective for VSA processes, whereas low Al content faujasites perform better at PSA conditions. Remarkably, present work best results clearly improve Faujasite 13X VSA–PSA performances, so far considered the industrial reference in absence of water. Moreover, combined VPSA processes, in terms of working capacity and adiabatic work required for compression/expansion, have also been studied, showing that VPSA systems are more efficient than pure PSA/VSA, for structures with intermediate Al content. Finally, an improved methodology has been derived, where GCMC mixture isotherms and energetic cost calculations are combined, and a more accurate way of estimating working capacities and breakthrough times is proposed. This new approach allows more realistic evaluations of adsorbents' performances, than those found in the literature based on pure adsorption data.

1. Introduction

Carbon dioxide (CO_2) is the primary greenhouse gas generated by human activities, mainly from the combustion of fossil fuels (*e.g.,* oil, coal and natural gas) for energy and transportation [1]. Economic growth and industrial development are responsible of the increasing amount of atmospheric CO_2, and thus the resulting global warming and climate change that have attracted increasing attention in the last years [2,3].

Despite the development of alternative renewable energy sources, fossil fuels still dominate in almost all near future energy projections. Therefore, many efforts have been addressed to the development of cost-efficient technologies for separation and capture of carbon dioxide [4,5], focusing on improved Carbon Capture and Sequestration/Utilization (CCS/U) processes. The aim is to capture CO_2 emissions, and either reuse or store it, so it will not enter into the atmosphere. Moreover, these technologies should satisfy low cost energy requirements [6,7].

Post-combustion power plants constitute the largest stationary source of CO_2 emissions. Concerning coal-fired plants, the largest flue gas components in dry weight by volume are N_2 (75–80%), CO_2 (15–16%) and O_2 (4–5%), with total pressures near 100 kPa and temperatures between 40 and 60 °C (*i.e.*, 313–333 K) [8]. Aqueous amine solutions are currently the most viable absorbents for carbon capture, under the aforementioned conditions, being monoethanolamine (MEA) in water the benchmark solvent against which competing technologies are generally compared. The low solvent cost and proven effectiveness make MEA an attractive absorbent for many applications. However, it suffers from high parasitic energy consumption, over 30%, as well as adverse environmental impact, in the form of solvent losses and corrosion issues [9–11].

Alternative technologies, aimed at mitigating some of the disadvantages of these amine solutions, are an active area of research. Solid adsorbents are promising candidates, since they may reduce the energy required for regeneration, according to

* Corresponding author.
E-mail address: gamallo@ub.edu (P. Gamallo).

http://dx.doi.org/10.1016/j.jcou.2017.03.007
2212-9820/

Nomenclature

b	Constants in the Langmuir-Freundlich equation for component A ($kPa^{-\upsilon}$)
BTC	Benzene-1,3,5-tricarboxylate
C	Ideal gas concentration at the feeding-gas conditions ($kmol\,m^{-3}$)
CCS/U	Carbon capture and sequestration/utilization
EOS	Equation of state
FAU	Faujasite
GC	Grand canonical
GCMC	Grand canonical monte carlo
IAST	Ideal adsorbed solution theory
L	Length of packed bed (m)
LJ	Lennard-Jones
LSX	Low silica x
LTA	Linde type a
MC	Monte carlo
MEA	Monoethanolamine
MOF	Metal organic framework
N	Amount adsorbed per mass of adsorbent ($mol\,kg^{-1}$)
NIST	National Institute of Standards and Technology
$N_{k,sat}$	Maximum loading (saturation) of component a ($kmol\,m^{-3}$)
P	Pressure (kPa)
PSA	Pressure swing adsorption
q_i	Partial charge of atom i
q_{ST}	Isosteric heat of adsorption at infinite dilution ($kJ\,mol^{-1}$)
R	Gas constant ($8.314\,kPa\,m^3\,kmol^{-1}\,K^{-1}$)
r_{ij}	Distance between a pair of atoms i and j (m)
$S_{A/B}$	Selectivity
t	Time (s)
T	Temperature (K)
TSA	Temperature swing adsorption
u	Superficial gas velocity ($m\,s^{-1}$)
U_{ij}	Potential energy between a pair of atoms i and j ($kJ\,mol^{-1}$)
U_g	Total potential energy of an isolated guest molecule ($kJ\,mol^{-1}$)
V	Total volume of packed bed (m^3)
VOC	Volatile organic compounds
VPSA	Volume pressure swing adsorption
VSA	Volume swing adsorption
W	Adiabatic energy requirement for compression/vacuum (kJ)
WC	Working capacity of the targeted component in the mixture ($mol\,kg^{-1}$)
x_A	Mole fraction of component a in the adsorbed phase
y_A	Mole fraction of component a in the gas (bulk) phase
z	Distance along the adsorber (m)

Greek symbols

ε	Voidage of bed
ε_{ij}	Lennard-Jones potential well depth ($kJ\,mol^{-1}$)
ε_0	Vacuum permittivity ($F\,m^{-1}$)
κ	Polytropic parameter of gases
η	Feeding/vacuum blower efficiency
ρ_S	Framework density ($kg\,m^{-3}$)
σ_{ij}	Lennard-Jones potential diameter (m)
τ	Time necessary per saturation in a cycle [adim.]
μ	Chemical potential ($kJ\,mol^{-1}$)
ν	Intersticial gas velocity ($m\,s^{-1}$)

Subscripts

ads/feed	Adsorption or feeding conditions
des/regen	Desorption or regeneration conditions
k	Species in the gas mixture ($k = A, B, C, \ldots$)

their properties. This step is typically accomplished by Swing Adsorption processes, where desorption is performed by a) decreasing the pressure (Pressure Swing Adsorption, PSA, or Vacuum Swing Adsorption, VSA), b) increasing the temperature (Temperature Swing Adsorption, TSA) or c) by application of electrical current (Electric Swing Adsorption, ESA). All these processes are considered viable economic and ecological possibilities, and indeed numerous examples of commercial gas separation/purification processes, such as air fractionation, hydrogen production, carbon dioxide capture and volatile organic compounds (VOC) removal are already available, to name a few [12–17]. Focusing on pressure swing processes, the feeding gas system in VSA operates at a pressure one order of magnitude lower than in PSA air compressor, resulting in significant energy savings, because higher pressures are directly proportional to higher energy consumption [18,19].

Finding the most efficient adsorbents has attracted both experimental and theoretical research focus, and even new adsorbent materials are being synthesized in the large scale, claiming suitability for post-combustion CO_2 capture [10,20]. Zeolites, activated carbons, silicas and metal−organic frameworks (MOFs) have received significant attention as alternatives to amine solutions, demonstrating high CO_2 capacities and high selectivities for CO_2 over N_2, together with reduced regeneration energy penalties [9,21–23]. It is known that traces of water vapour in the post-combustion flow drastically reduce the CO_2 adsorption in zeolites, whereas activated carbons present good performance even in presence of water [21,24]. This fact makes an additional step for moisture removal prior to CO_2 adsorption mandatory in the case of zeolites.

Adequate, long–lasting capture materials should fulfil two main conditions. First, a potentially practical adsorbent should possess good adsorption capacity, high selectivity, as well as improved working capacity and regenerability, among other properties [11,25,26]. Second, it should be highly air-stable and be able to maintain its stability over multiple cycles [27]. Among these materials, zeolites look especially adequate because of their narrow and uniform pore size, high surface area, adjustable hydrophobic and hydrophilic nature, ion exchange capacity and strong acidity. They are frequently used in PSA and VSA processes for removing CO_2 from air, as an impurity, because of their high CO_2 selectivity [28,29]. Moreover, they offer a much better thermal and mechanical stability than other adsorbent materials recently described in the literature, such as MOFs, even though the latter possess higher pore volumes and surface areas [30,31].

Zeolites are molecular sieves with a 3D framework structure built from TO_4 tetrahedrals (T denotes tetrahedral–coordinated Si, Al, P, etc), possessing orderly distributed micropores with diameters smaller than 2 nm. Although all zeolite families are constructed from TO_4 tetrahedra, the different ways in which they can be connected lead to a rich variety of zeolite structures [32–34]. Dehydrated faujasite (FAU)-type structures are a family of zeolites built from silicon, aluminium and oxygen atoms, with a composition that depends on the Si/Al ratio, $(Na,Ca_{1/2},Mg_{1/2})_nAl_nSi_{192-n}O_{384}$, $0 \le n \le 96$ [35]. They consist of b-cages and hexagonal prisms, connected in such a manner that large internal supercages are created. The properties of the faujasites depend on the nature, number and distribution of the framework cations. As the Si/Al ratio increases, the cation content decreases, the thermal stability is higher, the surface becomes more hydrophobic and the

zeolite loses its catalytic properties. That is of supreme importance in the evaluation of energetic costs for the CO_2 capture and, obviously, in the adsorbent material regenerability [36]. Thus, FAU-type zeolites present outstanding properties for their use in adsorptive separations. Furthermore, their open three-dimensional pore system results in much faster intra-crystalline diffusion rates as compared to other zeolites [37].

In this work, the influence of the Si/Al-ratio in FAU zeolites, with sodium exchanged cations, on the gas adsorption behaviour for post-combustion CO_2 capture and separation in PSA and VSA processes, has been evaluated in detail. Ten faujasite structures with different Al content have been considered, which makes it the most extensive study to date. A more complete understanding of the separation mechanism has been gained from complementary methods, including transient breakthrough simulations, as well as an extensive analysis regarding the effect of operating conditions in capture costs. Positive results indicate that the present methodology may serve as a useful tool for adsorbent materials screening and design.

The paper is organized as follows: structure details and computational methodology are described in Section 2. Results for all the different structures are presented in Section 3, being divided in four topics: a) simulations for pure components, b) results for ternary mixtures, c) evaluation of their performance in PSA and VSA units (focusing on working capacities, energetic requirements and transient breakthrough simulations) and d) combined VPSA processes. Finally, the main conclusions are summarized in Section 4.

2. Methods and computational details

2.1. Faujasite structures

In this work, molecular simulations have been performed as a screening tool for choosing the most efficient adsorbent material among ten FAU-type structures with different Si/Al ratio (*i.e.*, containing sodium atoms as non-framework cations). These structures have been labelled as *n*-FAU, where n represents the number of aluminium or sodium atoms per unit cell, $n = 0, 6, 12, 24, 32, 48, 64, 77, 88$ and 96. These values correspond to Si/Al ratios of $+\infty$, 31, 15, 7, 5, 3, 2, 1.5, 1.2 and 1, respectively. FAU-type zeolites can be labelled either X or Y, depending on their framework aluminium density: X zeolites contain between 77 and 96 aluminium atoms per unit cell, whereas Y zeolites contain less than 77 aluminium atoms. Moreover, when the number of aluminium atoms per unit cell is greater than 88 the Si/Al ratios are lower than 1.15 and the faujasite is usually called a Low Silica X zeolite (LSX) [38]. The *n*-FAU structures with $n \neq 88$ were obtained from 88-FAU (commonly named zeolite 13X), by randomly replacing aluminium by silicon atoms and satisfying the generally accepted Löwenstein's avoidance rule [39], which states that Al-O-Al bonds cannot be found in the zeolitic framework. For the 88-FAU structure we use the atomic crystallographic position reported by Olson et al. [35] with a cubic unit cell of $a = b = c = 25.10$ Å.

Several random structures can be obtained satisfying the desired Si/Al ratio, and therefore different frameworks were constructed for each structure, finding that the distribution of Al atoms does not change considerably the main properties of the adsorbate. All FAU frameworks were treated as rigid structures with atoms fixed at their crystallographic positions. In addition, it is known that the mobility of the non-framework cations has a strong effect on the adsorption behaviour [40,41]; thus in our case the negative charge was counterbalanced by sodium atoms which were allowed to move freely along the FAU structure, adjusting their position depending on their interactions with the framework atoms, other sodium cations and the gas molecules. This represents a step further with respect to other works published in literature, in which the position of the cations is optimized, then frozen before running the GCMC simulation [10,41,42–45].

2.2. Force field and GCMC simulations

GCMC simulations exchange atoms or molecules with an imaginary ideal gas reservoir at a constant temperature *T*, volume *V* and chemical potential μ [46] Then, the amount of molecules adsorbed is calculated using a statistically averaged approach after the equilibrium stage for every single pressure point, allowing the construction of adsorption isotherms. All simulations were performed by means of LAMMPS code [47]. At every simulation step, the code attempts a number of GCMC exchanges (*i.e.*, insertions and deletions) of gas molecules between the simulation box and the imaginary reservoir, and a number of Monte Carlo movements (*i.e.*, translations and rotations) of gas molecules within the simulation box. Regarding MC exchanges, deletions and insertions were attempted with equal probability to ensure microscopic detailed balance whereas MC movements were also attempted with 50% probability. Finally, once the molecules are moved in a simulation step, an extra MC translation movement is attempted for the sodium cations. At least 4×10^6 MC equilibration steps and 8×10^6 MC production steps were used at each pressure condition.

Both pure-component and mixture isotherms were computed at 313 K, in a pressure range between 1 and 5000 kPa (except for pure CO_2 adsorption, where the pressure range was increased to 0.01–5000 kPa due to its high affinity with the adsorbent material even at very low pressures). According to the typical post-combustion gas composition, we considered the following ternary mixture in our simulations: CO_2 (15%), N_2 (80%) and O_2 (5%). As described below in Section 3.2, there is a significant lack of adsorption data reported in the literature for mixtures with more than two components. We assume that water and impurities have been previously removed from the tail gas in an earlier stage. This previous phase can be achieved using activated carbons for sulphur compounds and trace contaminant removal, silica gels for light hydrocarbon elimination, and activated aluminas, bauxite, and also silica gels for dehumidification [48].

The Peng-Robinson Equation of State (EOS) [49] was used to relate the pressure to the chemical potential required in the GCMC simulations. Pure substance parameters of the EOS were taken from the NIST database [50]. For the ternary mixtures, the van der Waals one-fluid mixing rule was used [51], and the binary parameters were taken from Vrabec et al. [52]

A potential model for CO_2, N_2 and O_2 molecules was used with rigid geometrical structures, where only the nonbonded interactions were taken into account. Moreover, we have excluded the pairwise interactions between the framework atoms, since the structure was treated as frozen, in order to save unnecessary computation time. Hence, at each simulation step, the total energy of the system was calculated as the sum of the adsorbate-faujasite and the adsorbate–adsorbate interaction energies, written as a sum of nonbonded interatomic terms modelled as a combination of Lennard Jones (LJ 12-6) and Coulomb potentials,

$$U_{ij} = 4\varepsilon_{ij}\left[\left(\frac{\sigma_{ij}}{r_{ij}}\right)^{12} - \left(\frac{\sigma_{ij}}{r_{ij}}\right)^{6}\right] + \frac{1}{4\pi\varepsilon_0}\frac{q_i q_j}{r_{ij}} \quad (1)$$

where U_{ij} is the potential energy between a pair of atoms *i* and *j* at a distance r_{ij}; q_i, q_j are the partial charge of atom *i* and *j*, respectively, ε_{ij} and σ_{ij} are the LJ potential well depth and diameter, respectively, and ε_0 is the vacuum permittivity. All the LJ and Coulomb parameters were taken from the force field developed by Calero's group [53,54]. These parameters have been proved to

accurately reproduce the experimental adsorption properties for pure CO_2, N_2 and O_2 molecules (among others) in many different zeolite framework types, at cryogenic and high temperatures. Moreover, it is applicable to all possible Si/Al ratios in a transferable manner, with sodium atoms as extra-framework cations.

Coulombic interactions were computed using the Ewald summation method [46] with a relative precision of 10^{-6}, LJ cutoff ratio was fixed at 12 Å, and van der Waals interactions between molecules were obtained from Lorentz-Berthelot mixing rules. Section I in the Supplementary information (SI) summarizes the Coulombic charges and LJ parameters used in this work, as well as the agreement between simulations and experimental data for selected structures (when available).

2.3. Parameters/Indicators for separating processes

The isosteric heat of adsorption of component A, $q_{st,A}$, is one of the most important thermodynamic quantities for understanding the thermal effects related to adsorption and the cost of desorption/regeneration. It provides information about the energy released during the adsorption process, and it depends on the temperature and surface coverage. From energy/particle fluctuations in the GC ensemble, the isosteric heat can be calculated as [55]:

$$-q_{st,A} = \frac{< U \times N > - < U >< N >}{< N^2 > - < N >^2} - < U_g > - RT \quad (2)$$

where U is the total potential energy of the system per molecule, N is the number of molecules adsorbed, U_g is the energy of an isolated guest molecule and the brackets $< \ldots >$ denote an average in the GCMC ensemble.

A helpful indicator for the mixture separation ability is the adsorption selectivity of a porous adsorbent. This selectivity ($s_{A/B}$) for component A relative to B species, is calculated as:

$$s_{A/B} = \left(\frac{x_A}{x_B}\right)\left(\frac{y_B}{y_A}\right) \quad (3)$$

where x_A and x_B are the molar fractions of species A and B in the adsorbed phase, respectively, while y_A and y_B correspond to the molar fractions of A and B in the bulk phase (*i.e.*, feeding conditions), respectively. In the present work selectivity values are obtained directly from the mixture GCMC simulations, instead from the pure isotherm data, as it is usually done in both theoretical [56–58] and experimental [15,16,29,43,59–61] works published in literature.

Apart from the adsorption selectivity, another very important property that is often used as evaluation criteria in Swing Adsorption processes is the working capacity (WC_A) of the targeted component in the mixture. This quantity is defined as:

$$WC_A = N_{A,ads} - N_{A,des} \quad (4)$$

where A is the targeted component (*i.e.*, CO_2) and $N_{A,ads}$ and $N_{A,des}$ are the uptake per mass of adsorbent under adsorption or feeding and desorption or regeneration conditions, respectively.

The working capacity is generally more relevant than the total uptake at the adsorption pressure, since it really determines the amount of A that can be recovered at each adsorption cycle. Thus, $N_{A,ads}$ corresponds to the CO_2 uptake obtained from the ternary mixture isotherms at the adsorption pressure (*i.e.*, 1000–3000 kPa and 100 kPa for PSA and VSA, respectively), whereas $N_{A,des}$ corresponds to the CO_2 uptake in the mixture obtained at the desorption step, which is more concentrated in CO_2 than the original flue gas mixture. When the material is highly selective for one component of the mixture, a good approximation is assuming pure gas recovered at the outlet of the adsorber, as have been implemented by several authors [15,62,63]. In that case, the amount of A removed from the adsorbent material is obtained from pure isotherms. However, in the present study, since carbon dioxide recovered is not completely pure, we have calculated the amount of remaining CO_2 in the adsorbent material (*i.e.,* at the desorption step) by multiplying the pure CO_2 uptake at desorption pressure by a fractional factor obtained from the composition in the adsorbed phase (using mixture isotherms data) and the molecules retained in the void volume within the adsorbent material.

There are other indicators for comparing adsorbent materials such as the Adsorption Figure of Merit [64], the solvent selection parameter [65], or the adsorbent productivity [66]. However, the first two indicators seem to be an empirical rule of thumb that works well for certain objectives, whereas the last indicator cannot be obtained from GCMC simulations that only allows getting equilibrium properties.

2.3.1. Packed bed adsorber breakthrough simulation methodology

It has been demonstrated that neither highest $s_{A/B}$ nor maximum WC_A on their own can be chosen as final criteria for adsorbent selection. However, it is the combination of them, which leads to the best adsorbent material, and also to determine the optimum energetic cost of CO_2 capture in PSA and VSA processes [11,31,67,68]. Breakthrough calculations mimic the dynamic conditions of a large-scale separation, and therefore they can be helpful to screening a variety of adsorbents for a specified separation and to evaluate the separation performance [69,70]. In this regard, it is recommended to analyse the transient breakthrough curves of gas mixtures at the outlet of the adsorber [71].

Assuming a plug flow model for the gas mixture through the fixed bed, maintained under isothermal conditions and negligible pressure drop, the composition at any position and instant of time can be obtained by performing material balances for the adsorbates, that is, by solving the partial differential Eq. (5) for each one of the k species in the gas mixture ($k = A, B, C, \ldots$).

$$\varepsilon\frac{\partial P_k}{\partial t} + (1-\varepsilon)RT\rho_S\frac{\partial N_k}{\partial t} + \frac{\partial(v \cdot P_k)}{\partial z} = 0 \quad (5)$$

In Eq. (5), the terms represent the accumulation of the adsorbate in the fluid phase, the rate of adsorption with time, and the convective flow of the adsorbate within the bed, respectively. Note that with these assumptions, intracrystalline diffusion term is negligible, and therefore, thermodynamic equilibrium prevails everywhere within the bed. Further details of the adsorber model, along with the numerical procedure used, are provided in earlier works [72–74]. Moreover, in Eq. (5), t is the time, z is the distance along the adsorber, ρ_S is the framework density, ε is the bed voidage that is the ratio of the void volume to the total volume of the bed, v is the interstitial gas velocity equal to the superficial gas velocity, u, divided by ε, and P_k the partial pressure of k-th component. Finally, the molar loadings of the species, $N_k(z,t)$, at any position and time were determined according to the Ideal Adsorbed Solution Theory (IAST) exhibited by Myers and Prausnitz [75]. The accuracy of IAST for estimating the mixture equilibrium in zeolites has been well established in literature [56].

In order to apply IAST, the excess component loadings of the pure isotherms were fitted with a Langmuir–Freundlich adsorption isotherm model,

$$N_k = \frac{N_{k,sat} b_k P_k^{v_k}}{1 + b_k P_k^{v_k}} \quad (6)$$

with $N_{k,sat}$ (kmol m^{-3}) and b_k (kPa$^{-\nu_k}$) standing for the adsorption constants of component k, and P_k the partial pressure of k-th component.

For a chosen purity of 0.5% CO_2 in the gaseous mixture exiting the adsorber, a breakthrough time (τ_{break}) was determined; this time controls the frequency of required regeneration and influences the working capacity of PSA or VSA units.

2.4. Techno-economic aspects

Isothermal PSA and VSA processes were simulated including only two fixed beds at constant temperature in parallel, according to the simplest scheme configuration. While one bed is adsorbing, the other bed is desorbing at a lower pressure. This is called Skarstrom's [76] four-step cycle, and it was selected as the baseline analysis in the present study. The shortcut method described by Chung et al. [77] was adopted for the calculations, since it is able to easily describe the characteristics of the PSA and VSA processes, including the effect of different operating conditions. The model classifies the four steps of the Skarstrom's cycle into two main groups: pressurization (step I) and adsorption (step II) are merged into "adsorption" group, while depressurization/blowdown (step III) and evacuation (step IV) are grouped into "desorption".

Desorption pressures between 5 and 10 kPa were assumed for the VSA processes, since it has been shown that these conditions can be achievable in experiments [78]. Conversely, for the high-pressure feeding operation (*i.e.*, PSA), we assumed that the desorbed stream is expanded from 1000 to 3000 kPa to atmospheric pressure.

In order to determine the energy requirements to capture and separate an amount of CO_2, it is required to calculate the work done during one cycle, involving pressurizing during adsorption step (for PSA) and vacuum during desorption step (for VSA). Therefore, the adiabatic energy requirement was calculated in a similar way of that presented by Chaffee et al. [79] and Riboldi et al. [80] using the following equations,

$$W_{feed}(kJ) = \left(\frac{k}{k-1}\right)\frac{RT}{\eta}\int_{t=0}^{t=\tau}\left(\varepsilon v_o C_{feed} + \frac{WC_{CO_2}}{y_{CO_2}^{feed}}\rho_S V(1-\varepsilon)\right)\left[\left(\frac{P_{feed}}{P_{atm}}\right)^{\frac{k-1}{k}} - 1\right]dt \quad (7)$$

$$W_{vacuum}(kJ) = \left(\frac{k}{k-1}\right)\frac{RT}{\eta}\int_{t=0}^{t=\tau}\left(\varepsilon v_o C_{feed} + N_{TOT}^{ads}\rho_S V(1-\varepsilon)\right)\left[\left(\frac{P_{atm}}{P_{vacuum}}\right)^{\frac{k-1}{k}} - 1\right]dt \quad (8)$$

where $\eta = 0.85$ (feeding/vacuum blower efficiency), k is the polytropic parameter that depends on the purity of the gas ($k = 1.28$ and 1.4 for pure CO_2 and air, respectively), τ is the time necessary per cycle, P_{atm} is the atmospheric pressure (*i.e.*, 101.375 kPa), P_{feed} corresponds to the instantaneous discharge pressure (kPa) from the feeding compressor and P_{vacuum} is the instantaneous pressure (kPa) to the vacuum pump. The term $\varepsilon v_o C_{feed}$ stands for the non-adsorbed molecules placed at the void spaces of the bed, where $\varepsilon = 0.4$ is the void fraction, C_{feed} is the concentration at the feeding conditions in kmol m^{-3} units, and v_o the velocity of the gas mixture through the bed in m s^{-1} units.

Depending on whether PSA or VSA processes are considered, the amount of pressurized or expanded substance differs. In VSA, the complete bed is subjected to a vacuum; hence the total amount adsorbed (N_{TOT}^{ads}) plus the molecules in the void space must be evacuated. Conversely, for PSA, the amount compressed will be higher and mainly depends on the working capacity of CO_2 at the feeding stream conditions, since purge has not been taken into account in this study.

3. Results and discussion

In this section, the main results for the ten different faujasite structures are presented and compared with other adsorbents for potential applications in post-combustion CO_2 capture, such as the Ca-A zeolite, and the Mg-MOF-74 and Cu-BTC metal organic frameworks. Pure component data and selectivities for these structures have been obtained from the works of Bae et al. (Ca-A) [15], Mason et al. (Mg-MOF-74) [16] and Bahamon et al. (Cu-BTC) [81]. Working capacities and CO_2 purities have been estimated from IAST calculations by fitting the pure component adsorption isotherms.

3.1. Pure components

The pure component adsorption isotherms for CO_2 on the different adsorbents evaluated are presented in Fig. 1. The corresponding fitting parameters used later for the costs evaluation are given in Section II in the SI. In all cases, the amount of CO_2 adsorbed or uptake is significantly higher at lower pressures than that of N_2 and O_2 (see Section III in the SI), indicating good selectivity towards carbon dioxide, even at lower quantities of sodium atoms within the framework.

It is generally accepted that the separation ability for CO_2 increases when increasing the electrostatic field inside the zeolite cavities, which is mainly caused by the framework charge. This charge can be varied either by the nature of the charge compensating cations or by the Al content of the zeolite framework [28]. From Fig. 1 it is clear that the CO_2 adsorption capacities at

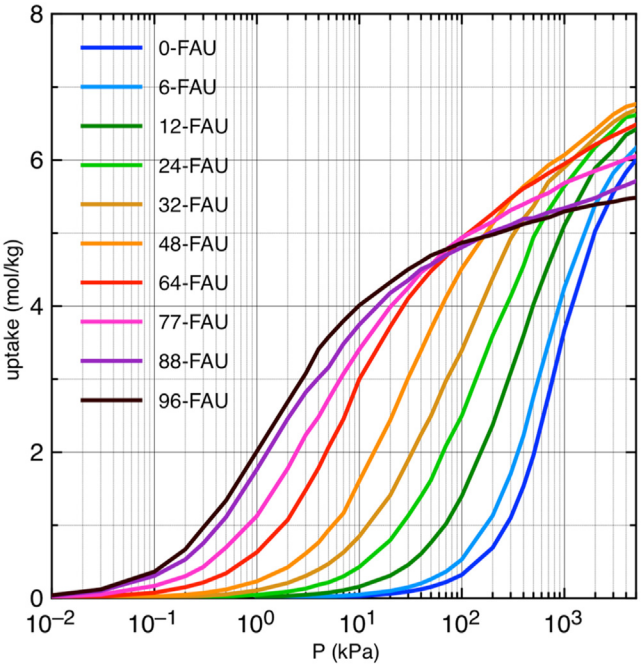

Fig. 1. CO_2 pure adsorption isotherms for ten different faujasite structures at 313 K. These structures have been labelled as n-FAU, where n is the number of aluminium or sodium atoms per unit cell. Lines are guide to the eyes, obtained from 29 equidistant single points for each structure. (For interpretation of the references to colour in this figure legend, the reader is referred to the web version of this article).

low–pressure regimes increase as the Al content does, indicating that the interaction between adsorbed molecules and the zeolite framework is stronger at high Na^+ contents. Thus, the 96-FAU structure is the first reaching saturation, whereas 0-FAU saturates the last. However, at high–pressure regimes the maximum adsorption capacity is found for structures having intermediate Al content, because the volume occupied by the cations inside the framework is not negligible, and the available pore volume for CO_2 adsorption diminishes as the Al content increases. Therefore, above 5000 kPa the maximum adsorption capacity is reached by the 48-FAU structure, whereas the most common industrially used structure 13X or 88-FAU shows a reduction of about 15% of the capacity with respect to the 48-FAU.

As above-mentioned, the isosteric heat of adsorption is an important point to be considered since the regenerability of the adsorbent material will depend on the CO_2-adsorbent interaction. A small q_{st} value implies better regeneration but lower adsorption capacity for a given pressure, and vice versa [29].

Fig. 2 shows the isosteric heat of adsorption for CO_2 as a function of the Al content. Due to the strong interaction between CO_2 molecules and the non-framework cations, the isosteric heat increases from 13 to 42 kJ mol^{-1} from the raw silica FAU to the 96-FAU zeolite, respectively. This fact has been also reported by A. Corma's group for LTA zeolites [29]. Interestingly, 96-FAU and Mg-MOF-74 show the same isosteric heat of adsorption (42 kJ mol^{-1}), and the same is observed comparing 12-FAU with Cu-BTC (25 kJ mol^{-1}). Finally, zeolite Ca-A exhibits the highest value (58 kJ mol^{-1}). The heats of adsorption remain more or less stable over the pressure range investigated for most of the structures, suggesting relatively homogeneous adsorption sites. This fact will not be discussed in more detail here as it has been previously discussed [82].

3.2. Mixture behaviour

Despite the large number of adsorbent materials that have been reported in the context of CO_2 capture, the main part of the studies has relied exclusively on pure CO_2 and N_2 isotherms. This fact makes the selection of the best materials for capturing CO_2 from an actual flue gas mixture challenging, since phenomena as co-adsorption and/or site competition are not taken into account. In addition, mixed gas adsorption measurements are often time-consuming, requiring carefully designed custom equipment and complex data analysis [83]. As a result, there is a significant lack of mixed gas adsorption data reported in the literature for mixtures with more than two components, even though many industrial gas separations involve multicomponent mixtures.

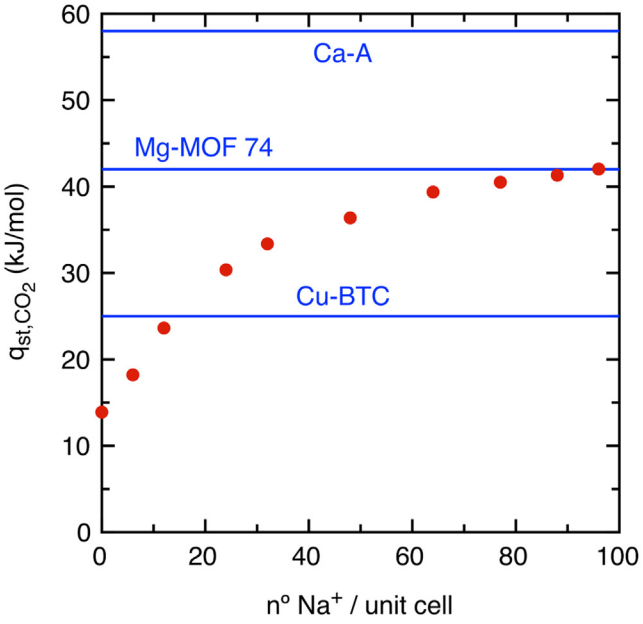

Fig. 2. Isosteric heat of adsorption for pure CO_2 at zero loading, as a function of the number of Na^+ cations per unit cell (red circles). The values for Ca-A, Mg-MOF-74 and Cu-BTC are also included as lines, for comparison, taken from the works of Bae et al. [15], Mason et al. [16] and Bahamon et al.[81], respectively.

Fig. 3 shows the adsorption isotherms at 313 K for carbon dioxide and nitrogen in four selected structures from both pure and mixture simulations, as well as the IAST mixture prediction. In this case, the *x* axis represents the total and partial pressure of *k-th* component at pure and mixture conditions, respectively. Oxygen data are omitted for the sake of clarity of the figures, but its loading is lower than that of nitrogen (see Section IV in the SI for complete isotherms).

As the amount of Na^+ ions in the structure increases, the behaviour of the CO_2 in mixtures mimic more consistently the adsorption isotherm at pure conditions, but the N_2 uptake in the mixture is much lower. IAST correctly predicts the N_2 behaviour in the mixture. However, for structures with intermediate and high Al content, the CO_2 uptake predicted by IAST is overestimated at high pressures and underestimated at low pressures (Fig. 3).

Fig. 4 shows the selectivity for CO_2 relative to N_2 for the ten structures evaluated over the entire range of pressures. As expected, 96-FAU has the highest CO_2 selectivity, ranging from 1150 to 170, at 5 and 5000 kPa, respectively, while 0-FAU has the lowest value, ranging from 4 to 6 in the same pressure range. The high selectivity values for NaX-type zeolites are even greater than those of Ca-A (250 at feeding conditions of 15 kPa CO_2, 75 kPa N_2 and 313 K) and Mg-MOF-74 (175 at feeding conditions of 15 kPa CO_2, 75 kPa N_2 and 313 K). Finally, Cu-BTC selectivity is similar to that of 12-FAU (18 at feeding conditions of 14 kPa CO_2, 86 kPa N_2 and 318 K). It is worth mentioning that, for zeolites having 64 or more Na^+ cations per unit cell, the selectivity decreases as the pressure is increased. However, it remains constant for zeolites having between 12 and 48 Na^+ atoms, and even increases slightly with the pressure whether the number of Na^+ cations per unit cell is below 12. The reason of this decreasing in selectivity with pressure for zeolites having high Na^+ content is associated with the fact that these are the first structures in reaching CO_2 saturation and it obviously occurs since no more empty space is available for CO_2 molecules, although adsorption of smaller molecules like N_2 and O_2 is still possible.

3.3. Evaluation of PSA/VSA processes

Swing adsorption cycles and conditions can be manipulated to meet a variety of demanding requirements, for instance to provide high purity CO_2, or to minimize power demands [18,84,85]. Moreover, same working capacities can be obtained by changing the adsorption/desorption pressures (*i.e.*, feeding/regeneration steps); the one with the lowest compression costs would then be the best material. The aim of this section is to test different conditions and to be able of selecting, for each faujasite structure, those conditions that minimize both the power and capital costs for CO_2 capture.

Carbon dioxide working capacity for the different FAU structures are given in Fig. 5. Four operating conditions $P_{feed.}$-$P_{regen.}$ have been considered (two for each process), which correspond to 1000–100 and 3000–100 kPa for PSA, and 100–10 and 100–5 kPa for VSA. Note that for VSA process, desorption pressures above 10 kPa imply net values of working capacities of almost zero for most of the structures.

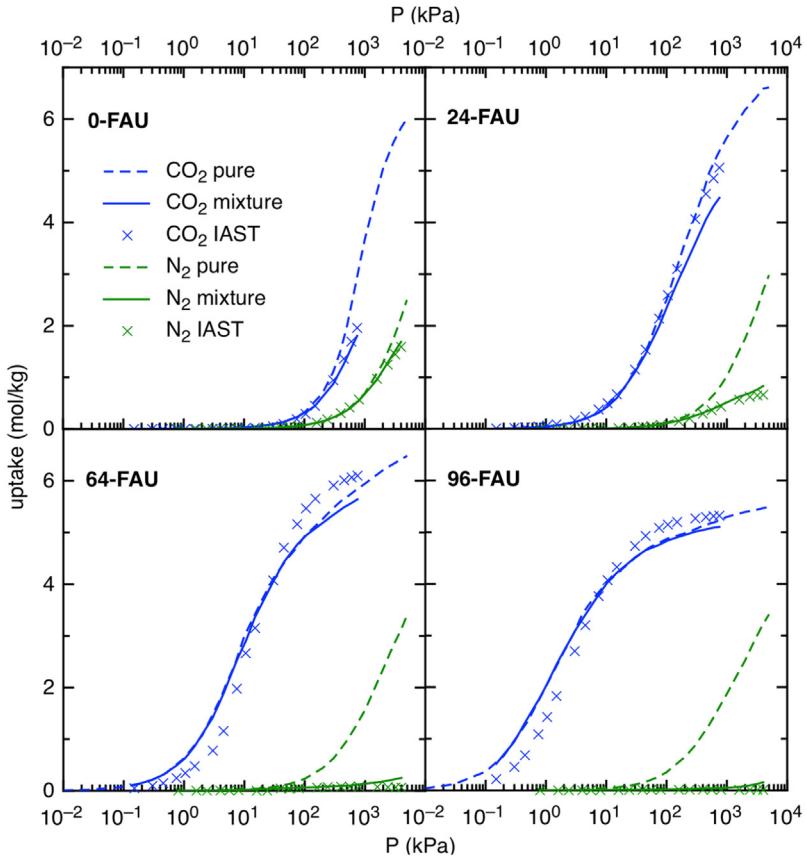

Fig. 3. Simulated adsorption isotherms for CO_2 (blue) and N_2 (green) for four selected faujasite structures at pure (dashed lines) and mixture (solid lines) conditions, at 313 K. IAST mixture prediction (cross marks) has also been included. The *x* axis represents the total and partial pressure of *k*-th component at pure and mixture conditions. (For interpretation of the references to colour in this figure legend, the reader is referred to the web version of this article.)

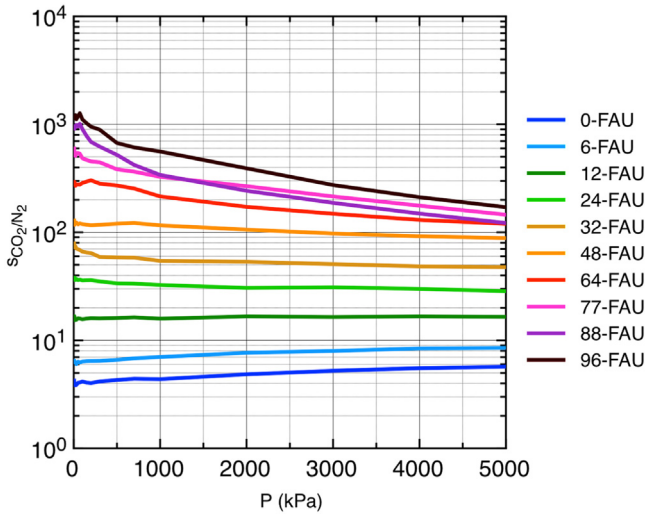

Fig. 4. Calculated selectivities for CO_2 relative to N_2 as a function of pressure, for ten different faujasite structures at 313 K. (For interpretation of the references to colour in this figure legend, the reader is referred to the web version of this article.)

Regarding the PSA process, the working capacity is almost tripled when the feeding pressure at adsorption conditions is raised from 1000 to 3000 kPa, for all the faujasite structures. Moreover, the NaY-type structures present higher working capacities than the NaX-type structures, reaching optimum values at 12–24 Na^+ cations per unit cell. As saturation conditions are approached at high pressures, the hierarchy of WC_{CO2} is dictated largely by the pore volumes and free surface areas, which are greater for faujasites with low Al content since they present a lesser amount of Na^+ cations. While NaX-type faujasites showed highest uptakes, the number of CO_2 desorbed molecules at regenerating conditions (*i.e.*, 100 kPa) is small, making them rather less interesting for the PSA process. In contrast, NaX-type faujasites present good working capacities for the VSA process, especially when the pressure at the desorption conditions is lowered to 5 kPa. In fact, working capacities for 48-FAU and 64-FAU structures operating between 100 and 5 kPa are almost as high as the value of the Ca-A zeolite, which is around 1.55 mol kg^{-1}. Conversely, MOFs are the adsorbent materials with the highest working capacities at PSA conditions, because they saturate at much higher pressures. For instance, Cu-BTC and Mg-MOF-74 present values of 4.72 and 6.06 mol kg^{-1} operating between 3000 and 100 kPa, respectively, but their values become lower operating between 100 and 10 kPa (*i.e.*, 0.27 and 0.52 mol kg^{-1}). Finally, it is important to note that experimental materials are known to be not fully activated and then, some discrepancies could appear in their performance compared to simulated perfect crystals.

The CO_2 purity at outlet of the adsorber is an important variable to consider, especially when it is possible to reuse it for other applications. Fig. 6 shows the CO_2 purity (%) exiting the adsorber at the desorption step as a function of the PSA adsorption pressure and VSA desorption pressure for all the faujasite structures, assuming a packed bed with a total volume of 0.1 m^3 (*i.e.*, L = 0.1 m, A = 1 m^2) and a void fraction of $\varepsilon = 0.4$ (ε = (bulk density)/(framework density)). The final CO_2 purity depends on the selectivity, the working capacities for $CO_2/N_2/O_2$, and also on the

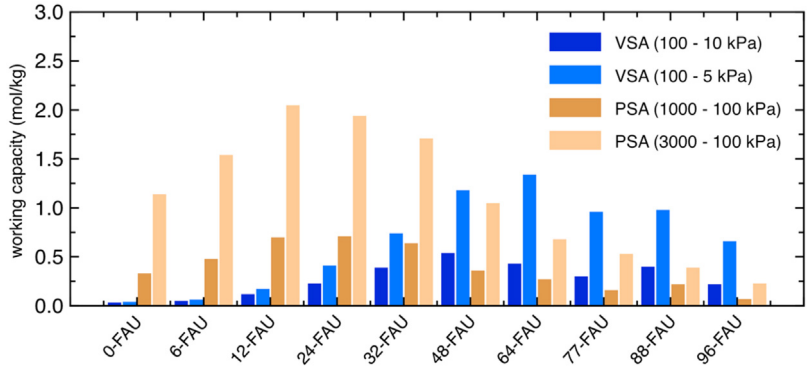

Fig. 5. Calculated CO_2 working capacities for the ten FAU structures considered corresponding to PSA and VSA processes at different $P_{feed.}$-$P_{regen.}$, and at 313 K. (For interpretation of the references to colour in this figure legend, the reader is referred to the web version of this article.)

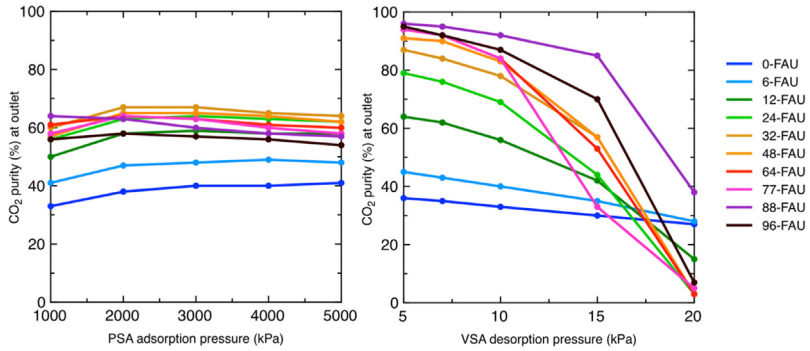

Fig. 6. CO_2 purity (%) in the gaseous mixture exiting the bed adsorber at the desorption step, as function of adsorption ($P_{feed.}$; PSA, left) and desorption ($P_{regen.}$; VSA, right) pressure, assuming a packed bed with a total volume of 0.1 m^3 (L = 0.1 m, A = 1 m^2) and a void fraction of $\varepsilon = 0.4$. Simulations performed at 313 K. (For interpretation of the references to colour in this figure legend, the reader is referred to the web version of this article.)

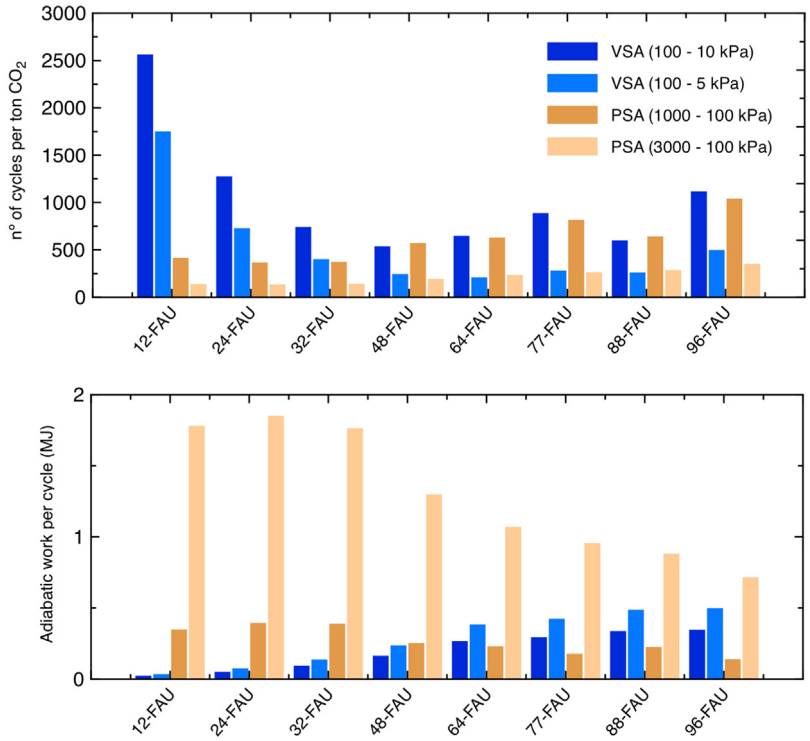

Fig. 7. Number of VSA and PSA cycles needed to remove a ton of CO_2 for each structure (up) and adiabatic work per cycle (down), assuming a packed bed with a total volume of 0.1 m^3 (L = 0.1 m, A = 1 m^2) and a void fraction of $\varepsilon = 0.4$. 0-FAU and 6-FAU structures have not been included for the clarity of the plot (the number of required PSA cycles is 7200 and 8300 for 6-FAU and 0-FAU, respectively). (For interpretation of the references to colour in this figure legend, the reader is referred to the web version of this article.)

void fraction ε. It can be seen that the VSA process allows obtaining a higher CO_2 purity than PSA ones, because the N_2 and O_2 working capacities in PSA conditions are much higher than in VSA conditions, as well as the amount of N_2 and O_2 in the empty space of the bed. Moreover, in general NaX-type structures drive to higher purities due to their high selectivity. Regarding the zeolite Ca-A, we have estimated, assuming also $\varepsilon = 0.4$, high purity values for VSA applications up to 98% at 100–5 kPa, similar to 88-FAU. However, for PSA application at 3000–100 kPa its value is only around 49%, overtaken by most of the faujasite structures considered. Finally, MOFs present lower CO_2 purity than most of the faujasite structures at VSA conditions (89% and 67% for Mg-MOF-74 and Cu-BTC, respectively) but higher than all zeolite structures at PSA process (87% and 63% for Mg-MOF-74 and Cu-BTC, respectively). Higher purity values can be achieved by reducing the void fraction or also by combining several Skarstrom cycles.

For PSA units operating at say 1000 kPa, the screening on the basis of $s_{CO2/N2}$ indicates 96-FAU as the best choice. If we use WC_{CO2} for ranking, then 12-FAU emerges as better choice. However, in terms of CO_2 purity, one should select the 88-FAU structure. A similar disagreement is also observed for VSA processes. This dilemma indicates the need to examine the PSA and VSA operations in more detail.

Fig. 7 shows the number of PSA ($P_{feed.}$ = 3000/1000 kPa) and VSA ($P_{regen.}$ = 10/5 kPa) cycles needed to remove a ton of CO_2 for each structure, and also the adiabatic work per cycle calculated by means of Eqs. (7) and (8), assuming a packed bed with a total volume of 0.1 m^3 and a void fraction of $\varepsilon = 0.4$. As the PSA feeding pressure is raised or the VSA regeneration pressure is decreased, the number of required cycles is lower, but the adiabatic work for pressurizing or swing to vacuum increases. A compromise must be found between a low number of cycles and a moderate energetic cost. Note that, as shown in Fig. 7 (bottom), decreasing the regeneration pressure in a VSA process from 10 to 5 kPa increases the adiabatic work per cycle by 40% approximately. However, Fig. 5 shows that the working capacities at 100–5 kPa are two or even three times greater than those at 100–10 kPa.

Fig. 7 also shows that for structures with low Al content the number of required VSA cycles is much higher than the number of required PSA cycles. Thus, using these structures under VSA conditions is unpractical. In contrast, structures with intermediate and high Al content require a similar number of VSA-100/5 and PSA-3000/100 cycles per ton of CO_2. However, the adiabatic work for compression is much higher than the adiabatic work for evacuating at these conditions, making them more interesting for a VSA process.

Note that in our model we only include operating costs for gas compression and evacuation at the desired pressures. We do not include capital costs of equipment and adsorbent materials. Therefore, we cannot establish a final ranking in terms of total capital costs. Moreover, the costs for previous dehumidification of the flue gas and the costs associated to post-separation (*i.e.,* compression and transport) should also be included for a full evaluation. According to the work by Leperi et al. [86] the operating costs represent close to 45% of the total requirements, while annualized capital costs around 5%, dehumidification around 10% and finally, post-compression and transport around 40%.

3.3.1. Breakthrough curves

Potentiality for CO_2 separation from the ternary mixture considered under dynamic conditions was also studied by simulated breakthrough experiments. The following parameters were used: length of packed bed, L = 0.1 m, (A = 1 m^2); voidage of packed bed, $\varepsilon = 0.4$; superficial gas velocity at inlet, $u = 0.04\ m\ s^{-1}$. When comparing among different materials, the fractional voidage was held constant, implying that the volumes of adsorbent materials used in the fixed bed are the same for all zeolites. Therefore, the total mass of the adsorbents used is governed by the framework density. The transient breakthrough simulation results are presented in terms of a dimensionless time (τ_{break}) defined by dividing the actual time (t) by the contact time, τ ($\tau = L\varepsilon \cdot u^{-1}$).

Fig. 8 presents the breakthrough times as a function of desorption or regeneration pressures, for both PSA and VSA processes. In these simulations, the working capacity of the materials has been taken into account considering saturation times from a non-clean bed, initially containing the quantity of molecules present at the desorption conditions from the previous cycle. An alternative way of performing the breakthrough simulations is considering as initial state a clean bed with no molecules within the framework. Several authors [15,16,61] commonly use the clean bed alternative, although it provides different results, with larger breakthrough times and clearly, resulting in a different adsorbent materials ranking. However, this alternative implies a system where, after each PSA or VSA cycle, a purge of the column is required to push the remaining CO_2 out of the column and hence, consuming a higher amount of energy. The comparison of breakthrough times obtained in both situations can be found in the Section V in the SI.

In PSA, the value of τ_{break} increases when increasing the adsorption pressure up to a maximum value around 1000–2000 kPa, and above that point it starts to decrease. The reason for this increment is because the working capacity of the material is increased as the pressure range is larger, and thus the time for reaching saturation becomes longer. However, at higher

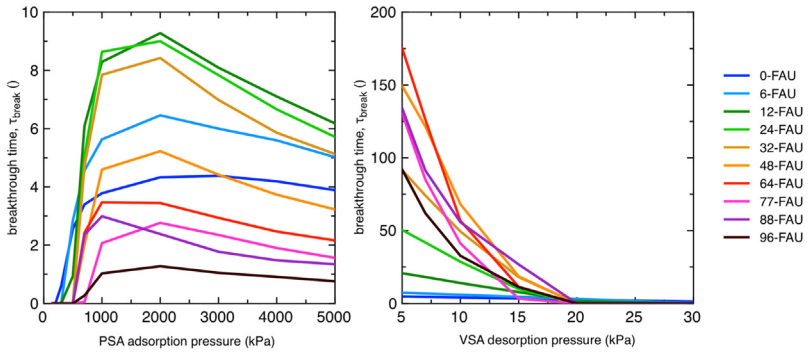

Fig. 8. Dimensionless breakthrough times for a chosen purity of 0.5% CO_2 in the gaseous mixture exiting the adsorber, as a function of adsorption (PSA, left side) and desorption (VSA, right side) pressures. Simulations performed at 313 K. (For interpretation of the references to colour in this figure legend, the reader is referred to the web version of this article.)

adsorption or feeding pressures, the adsorbent reaches saturation faster, and then an increment in the pressure range does not improve the working capacity, resulting in a lower τ_{break} value. On the other hand, in VSA the value of τ_{break} is increased when decreasing the regeneration pressure, due to the higher working capacity. For instance, if a VSA process is considered operating at 100–5 kPa, the following hierarchy for breakthrough times is obtained: 64-FAU > 48-FAU > 88-FAU > 77-FAU > 96-FAU > 32-FAU > 24-FAU > 12-FAU > 6-FAU > 0-FAU. This sequence demonstrates the better separation performance for faujasites with intermediate Al content at these conditions.

3.4. Combined VPSA processes

A convenient procedure for CO_2 adsorption could be a process in which the adsorption step takes place at moderate pressures above atmospheric conditions, where expensive compression units are not required, and desorption is performed under vacuum conditions in order to avoid heating systems [66]. This is called VPSA process, and it can have even more chances of commercial application because of the low energy demand. Fig. 9 shows the working capacity and the adiabatic work required for selected faujasite structures as a function of different $P_{feed.}/P_{regen.}$

We have selected 5 different pressure conditions ranging from 100/5 kPa (pure VSA) to 2000/100 kPa (pure PSA) in such a way that the $P_{feed.}/P_{regen.}$ ratio is constant. The reason is that the adiabatic cost of compression/expansion mostly depends on this ratio (as suggested by Eqs. (7) and (8)). It can be observed that the working capacity strongly depends on the selected conditions, with values up to 1.43–1.47 kg mol^{-1} for 24-FAU, 32-FAU and 48-FAU structures. In fact, at these conditions all three structures present higher working capacities than zeolite Ca-A, whose value at 400/20 kPa is around 0.77. Fig. 9 also shows that the separation performance for 24-FAU and 32-FAU structures operating at 1000/50 kPa is remarkably good, as well as for 48-FAU structure operating at 400/20 kPa. At these conditions, the ratio between working capacity and adiabatic cost for all the three structures is very high, with potential use in industrial applications. Moreover, it can be seen that the VPSA performance of the commonly used Faujasite 13X structure (here 88-FAU) is quite bad compared to previous ones. Apart from presenting a smaller working capacity, it requires more power consumption at these conditions. The main reason is that, for this structure, the total amount of moles adsorbed (N_{TOT}^{ads} in Eq. (8)) is very high. This increases the required adiabatic work for expansion, as seen in Fig. 9.

4. Conclusions

Results shown in the present work demonstrate the strong influence of faujasite Si/Al ratio on the post-combustion CO_2 capture by adsorption in dehumidified streams. Ten faujasite structures with different Al content have been evaluated in detail for potential application in Swing Adsorption processes, by computing both pure and mixture adsorption isotherms for CO_2, N_2 and O_2. Among the materials assessed, 96-FAU in which Si/Al ratio equals to 1, presents the highest selectivity towards CO_2 and

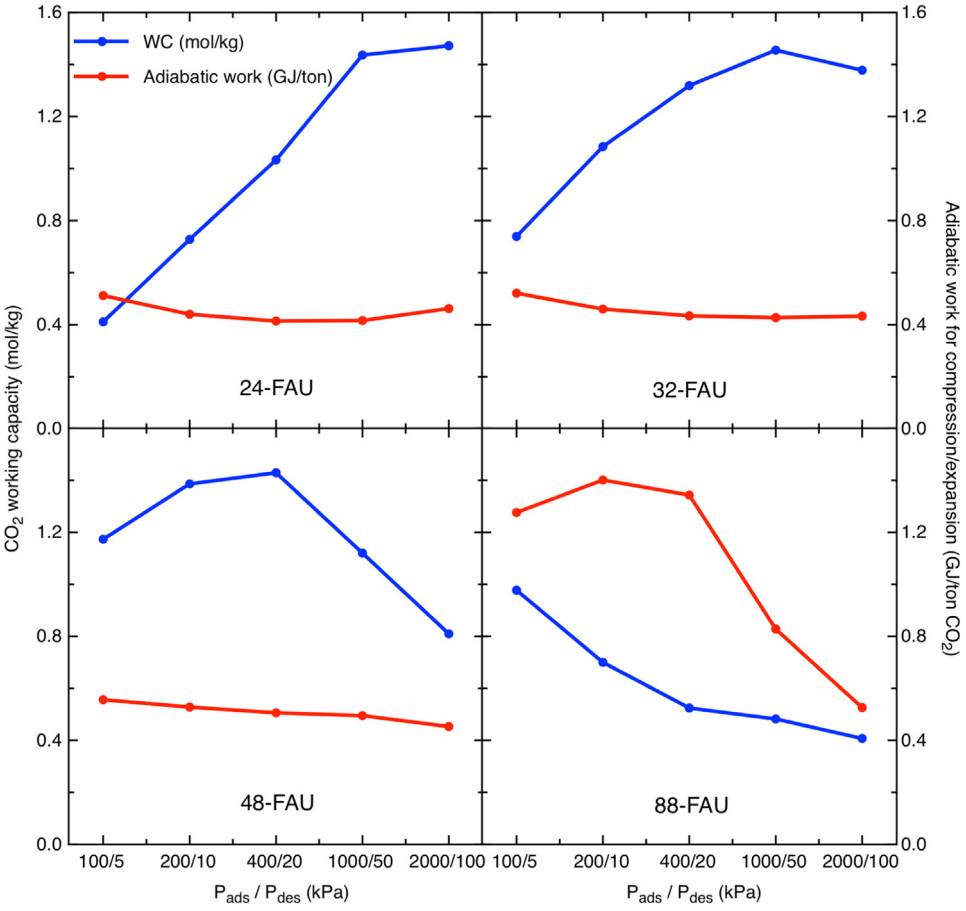

Fig. 9. Blue lines represent the CO_2 working capacity as a function of the VPSA adsorption ($P_{feed.}$) and desorption ($P_{regen.}$) pressures at 313 K. Red lines represent the adiabatic work required for compression/expansion (vacuum) to remove a ton of CO_2 assuming a packed bed with a total volume of 0.1 m^3 and void fraction of $\varepsilon = 0.4$. (For interpretation of the references to colour in this figure legend, the reader is referred to the web version of this article.)

isosteric heat of adsorption, but saturates at low pressures. Conversely, 0-FAU in which Si/Al ratio equals to ∞, presents the lowest selectivity and isosteric heat of adsorption, but allows capturing more CO_2 molecules at higher pressures. However, it turns out that structures with intermediate Al content present the greatest potential towards post-combustion CO_2 capture. Moreover, the potential separation of each structure strongly depends on the working range. For instance, in a VSA unit operating at 100–5 kPa (*i.e.*, $P_{feed.}$-$P_{regen.}$) 48-FAU and 64-FAU structures show the maximum working capacity, while in a PSA unit operating at 3000–100 kPa the best adsorbent materials in terms of working capacity are 12-FAU and 24-FAU structures. On the other hand, CO_2 purity at outlet of the adsorber may be an important variable, especially if it is necessary to reuse CO_2 in other applications. In this case, 88-FAU structure operating in a VSA system emerges as the better choice, with CO_2 purity up to 96%.

Dynamic breakthrough calculations for all the structures have been also computed both for PSA and VSA systems in a wide range of pressures. The breakthrough time obtained, that combines working capacity and selectivity, is considered as the final criterion for adsorbent selection. Our results confirm that 48-FAU and 64-FAU structures are the best adsorbent materials evaluated for VSA applications, while 12-FAU and 24-FAU structures are the top ones for PSA applications, in agreement with the analysis in terms of the working capacity.

Additionally, we have tested the separation performance for all the faujasite structures in different hybrid VPSA systems. The working capacity and the required adiabatic work for compression and expansion (vacuum) have been calculated for all structures at several pressure conditions, keeping constant the $P_{feed.}/P_{regen.}$ ratio at 20. In this way, we were able to determine which are the most optimal conditions for each structure (*i.e.*, high working capacities for low energy consumption). Our results show that 24-FAU, 32-FAU and 48-FAU present extremely good separation ability under VPSA conditions, outperforming by far the commonly used Faujasite 13X structure.

Finally, the present methodology allows the performance evaluation of different adsorbent materials at more realistic conditions than those found in literature. Selectivities and working capacities have been obtained from the ternary mixture adsorption isotherms, instead of pure adsorption ones. Additionally, for working capacity calculations, we have taken into account that at desorption conditions, the recovered CO_2 is not completely pure. Thus, instead of using the uptake at desorption pressure from the pure CO_2 adsorption isotherm, we calculate the real uptake at desorption conditions. Moreover, breakthrough simulations found in literature are usually computed starting from a clean bed with no molecules within the framework. However, at each PSA or VSA cycle, there is a remaining number of adsorbed molecules that are not desorbed during the desorption step. Thus, we have performed the dynamic breakthrough calculations by starting from a bed which already contains the quantity of molecules present at the desorption conditions. This model represents a further step for adsorbent selection and provides important guidelines for future screening and for designing novel materials.

Acknowledgments

Financial support to this research has been provided by the Spanish Ministry of Economy and Competitiveness (project number CTQ2014-53987-R) and, in part, from the Generalitat de Catalunya (project number 2014SGR1582). HPG thanks Generalitat de Catalunya for a predoctoral FI-DGR-2015 grant. PG thanks Generalitat de Catalunya for his Serra Húnter Associate Professorship. Computational resources provided by Consorci de Serveis Universitaris de Catalunya (CSUC, former CESCA) are gratefully acknowledged. With all the love PG wants to dedicate this study to his loved Pablo, Maria and Patricia, his best adsorbent materials.

Appendix A. Supplementary data

Supplementary data associated with this article can be found, in the online version, at http://dx.doi.org/10.1016/j.jcou.2017.03.007.

References

[1] D.Y.C. Leung, G. Caramanna, M.M. Maroto-Valer, An overview of current status of carbon dioxide capture and storage technologies, Renew. Sustain. Energy Rev. 39 (2014) 426–443.
[2] B.P. Spigarelli, S.K. Kawatra, Opportunities and challenges in carbon dioxide capture, J. CO_2 Util. 1 (2013) 69–87.
[3] N. MacDowell, N. Florin, A. Buchard, J. Hallett, A. Galindo, G. Jackson, C.S. Adjiman, C.K. Williams, N. Shah, P. Fennell, An overview of CO2 capture technologies, Energy Environ. Sci. 3 (2010) 1645–1669.
[4] R.M. Cuéllar-Franca, A. Azapagic, Carbon capture, storage and utilisation technologies: a critical analysis and comparison of their life cycle environmental impacts, J. CO_2 Util. 9 (2015) 82–102.
[5] N. Hedin, L. Andersson, L. Bergstrom, J. Yan, Adsorbents for the post-combustion capture of CO2 using rapid temperature swing or vacuum swing adsorption, Appl. Energy 104 (2013) 418–433.
[6] J. Čejka, H. van Bekkum, A. Corma, F. Schuth, Introduction to Zeolite Science and Practice, third ed., Elsevier, Amsterdam, 2007.
[7] S. Chu, Carbon capture and sequestration, Science 325 (2009) 1599.
[8] E.J. Granite, H.W. Pennline, Photochemical removal of mercury from flue gas, Ind. Eng. Chem. Res. 41 (2002) 5470–5476.
[9] K. Sumida, D.L. Rogow, J.A. Mason, T.M. McDonald, E.D. Bloch, Z.R. Herm, T.H. Bae, J.R. Long, Carbon dioxide capture in metal-organic frameworks, Chem. Rev. 112 (2012) 724–781.
[10] L. Lin, A.H. Berger, R.L. Martin, J. Kim, J.A. Swisher, K. Jariwala, C.H. Rycroft, A.S. Bhown, M.W. Deem, M. Haranczyk, B. Smit, In silico screening of carbon-capture materials, Nat. Mater. 11 (2012) 633–641.
[11] J.M. Huck, L. Lin, A.H. Berger, M.N. Shahrak, R.L. Martin, A.S. Bhown, M. Haranczyk, K. Reuter, B. Smit, Evaluating different classes of porous materials for carbon capture, Energy Environ. Sci. 7 (2014) 4132–4146.
[12] C.A. Grande, R.P.L. Ribeiro, E.L.G. Oliveira, A.E. Rodrigues, Electric swing adsorption as emerging CO2 capture technique, Energy Procedia 1 (2009) 1219–1225.
[13] R. Ribeiro, C.A. Grande, A.E. Rodrigues, Electric swing adsorption for gas separation and purification: a review, Sep. Sci. Technol. 49 (2014) 1985–2002.
[14] S. Sircar, Basic research needs for design of adsorptive gas separation processes, Ind. Eng. Chem. Res. 45 (2006) 5435–5448.
[15] T.H. Bae, M.R. Hudson, J.A. Mason, W.L. Queen, J.J. Dutton, K. Sumida, K.J. Micklash, S.S. Kaye, C.M. Brown, J.R. Long, Evaluation of cation-exchanged zeolite adsorbents for post-combustion carbon dioxide capture, Energy Environ. Sci. 6 (2013) 128–138.
[16] J.A. Mason, K. Sumida, Z.R. Herm, R. Krishna, J.R. Long, Evaluating metal-organic frameworks for post-combustion carbon dioxide capture via temperature swing adsorption, Energy Environ. Sci. 4 (2011) 3030–3040.
[17] M.A. Granato, T.J.H. Vlugt, A.E. Rodrigues, Molecular simulation of propane-propylene binary adsorption equilibrium in zeolite 13X, Ind. Eng. Chem. Res. 46 (2007) 7239–7245.
[18] D. Ko, R. Siriwardane, L. Biegler, Optimization of pressure swing adsorption and fractionated vacuum pressure swing adsorption processes for CO2 capture, Ind. Eng. Chem. Res. 44 (2005) 8084–8094.
[19] P. Xiao, J. Zhang, P. Webley, G. Li, R. Singh, R. Todd, Capture of CO2 from flue gas streams with zeolite 13X by vacuum-pressure swing adsorption, Adsorption 14 (2008) 575–582.
[20] I. Matito-Martos, A. Martin-Calvo, J.J. Gutierrez-Sevillano, M. Haranczyk, M. Doblare, J.B. Parra, C.O. Ania, S. Calero, Zeolite screening for the separation of gas mixtures containing SO2, CO2 and CO, Phys. Chem. Chem. Phys. 16 (2014) 19884–19893.
[21] N.A. Rashidi, S. Yusup, An overview of activated carbons utilization for the post-combustion carbon dioxide capture, J. CO_2 Util. 13 (2016) 1–16.
[22] J. Liu, P.K. Thallapally, B.P. McGrail, D.R. Brown, J. Liu, Progress in adsorption-based CO2 capture by metal-organic frameworks, Chem. Soc. Rev. 41 (2012) 2308–2322.
[23] Z. Zhang, Z.Z. Yao, S. Xiang, B. Chen, Perspective of microporous metal-organic frameworks for CO2 capture and separation, Energy Environ. Sci. 7 (2014) 2868–2899.
[24] J. Ling, A. Ntiamoah, P. Xiao, D. Xu, P.A. Webley, Y. Zhai, Overview of CO2 capture from flue gas streams by vacuum pressure swing adsorption technology, Austin J. Chem. Eng. 1 (2014) 1–7.
[25] Y. He, W. Zhou, R. Krishna, B. Chen, Microporous metal-organic frameworks for storage and separation of small hydrocarbons, Chem. Commun. 48 (2012) 11813–11831.
[26] Y.Q. Lan, H.L. Jiang, S.L. Li, Q. Xu, Mesoporous metal-organic frameworks with size-tunable cages: selective CO2 uptake, encapsulation of Ln3+ cations for luminescence, and column-chromatographic dye separation, Adv. Mater. 23 (2011) 5015–5020.

[27] H.L. Jiang, D. Feng, K. Wang, Z.Y. Gu, Z. Wei, Y.P. Chen, H.C. Zhou, An exceptionally stable, porphyrinic Zr metal-organic framework exhibiting pH-dependent fluorescence, J. Am. Chem. Soc. 135 (2013) 13934–13938.
[28] P.L. Llewellyn, G. Maurin, Chapter 17–Gas adsorption in zeolites and related materials, Stud. Surf. Sci. Catal. 168 (2007) 555–610.
[29] M. Palomino, A. Corma, F. Rey, S. Valencia, New insights on CO2-methane separation using LTA zeolites with different Si/Al ratios and a first comparison with MOFs, Langmuir 26 (2010) 1910–1917.
[30] R. Banerjee, A. Phan, B. Wang, C. Knobler, H. Furukawa, M. O'Keeffe, O.M. Yaghi, High-throughput synthesis of zeolitic imidazolate frameworks and application to CO2 capture, Science 319 (2008) 939–943.
[31] Y.S. Bae, R.Q. Snurr, Development and evaluation of porous materials for carbon dioxide separation and capture, Angew. Chem. Int. Ed. 50 (2011) 11586–11596.
[32] Y. Li, J. Yu, New stories of zeolite structures: their descriptions, determinations, predictions, and evaluations, Chem. Rev. 14 (2014) 7268–7316.
[33] M.E. Davis, Ordered porous materials for emerging applications, Nature 417 (2002) 813–821.
[34] C. Martínez, A. Corma, Inorganic molecular sieves: preparation, modification and industrial application in catalytic processes, Coord. Chem. Rev. 255 (2011) 1558–1580.
[35] D.H. Olson, The crystal structure of dehydrated NaX, Zeolites 15 (1995) 439–443.
[36] A. Corma, From microporous to mesoporous molecular sieve materials and their use in catalysis, Chem. Rev. 97 (1997) 2373–2420.
[37] D.M. Ruthven, Diffusion of linear paraffins and cyclohexane in NaX and 5A zeolite crystals, Zeolites 8 (1988) 472–479.
[38] I. Daems, P. Leflaive, A. Methivier, G.V. Baron, J.F.M. Denayer, Influence of Si:Al-ratio of faujasites on the adsorption of alkanes, alkenes and aromatics, Microporous Mesoporous Mater. 96 (2006) 149–156.
[39] W. Löwenstein, The distribution of aluminum in the tetrahedra of silicates and aluminates, Am. Mineral. 39 (1954) 92–96.
[40] S. Calero, D. Dubbeldam, R. Krishna, B. Smit, T.J.H. Vlugt, J.F.M. Denayer, J.A. Martens, T.L.M. Maesen, Understanding the role of sodium during adsorption: a force field for alkanes in sodium-exchanged faujasites, J. Am. Chem. Soc. 126 (2004) 11377–11386.
[41] A. Martin-Calvo, J.B. Parra, C.O. Ania, S. Calero, Insights on the anomalous adsorption of carbon dioxide in LTA zeolites, J. Phys. Chem. C 118 (2014) 25460–25467.
[42] A.O. Yazaydin, R.W. Thompson, Molecular simulation of water adsorption in silicalite: effect of silanol groups and different cations, Micropor. Mesopor. Mat 123 (2009) 169–176.
[43] R.S. Pillai, S.A. Peter, R.V. Jasra, CO2 and N2 adsorption in alkali metal ion exchanged X-Faujasite: grand canonical Monte Carlo simulation and equilibrium adsorption studies, Microporous Mesoporous Mater. 162 (2012) 143–151.
[44] G. Maurin, Y. Belmabkhout, G. Pirngruber, L. Gaberova, P. Llewellyn, CO2 adsorption in LiY and NaY at high temperature: molecular simulations compared to experiments, Adsorption 13 (2007) 453–460.
[45] W. Louisfrema, B. Rotenberg, F. Porcher, J.L. Paillaud, P. Massiani, A. Boutin, Cation redistribution upon dehydration of Na58Y faujasite zeolite: a joint neutron diffraction and molecular simulation study, Mol. Sim. 41 (2015) 1371–1378.
[46] D. Frenkel, B. Smit, Understanding Molecular Simulation: from Algorithms to Applications, Academic Press, London, 2002.
[47] S. Plimpton, Fast parallel algorithms for short-range molecular dynamics, J. Comp. Phys. 117 (1995) 1–19.
[48] J.A. Ritter, A.D. Ebner, Carbon Dioxide Separation Technology: R&D Needs for the Chemical and Petrochemical Industries, (2007) www.eere.energy.gov/manufacturing/pdfs/co2_separation_report_v2020.pdf, (accessed 05 September 2016).
[49] D.Y. Peng, D.B. Robinson, A new two-constant equation of state, Ind. Eng. Chem. Fundam. 15 (1976) 59–64.
[50] E.W. Lemmon, M.O. McLinden, M.L. Huber, NIST Thermodynamic Properties of Refrigerants and Refrigerants Mixtures Database (REFPROP), Version 7.0, (2002) .
[51] S.K. Shibata, S.I. Sandler, Critical evaluation of equation of state mixing rules for the prediction of high-pressure phase equilibria, Ind. Eng. Chem. Res. 28 (1989) 1893–1898.
[52] J. Vrabec, G.K. Kedia, U. Buchhauser, R. Meyer-Pittroff, H. Hasse, Thermodynamic models for vapor-liquid equilibria of nitrogen + oxygen + carbon dioxide at low temperatures, Cryogenics 49 (2009) 72–79.
[53] A. Garcia-Sánchez, C.O. Ania, J.B. Parra, D. Dubbeldam, T.J.H. Vlugt, R. Krishna, S. Calero, Transferable force field for carbon dioxide adsorption in zeolites, J. Phys. Chem. C 113 (2009) 8814–8820.
[54] A. Martin-Calvo, J.J. Gutiérrez-Sevillano, J.B. Parra, C.O. Ania, S. Calero, Transferable force fields for adsorption of small gases in zeolites, Phys. Chem. Chem. Phys. 17 (2015) 24048–24055.
[55] T.J.H. Vlugt, E. García-Pérez, D. Dubbeldam, S. Ban, S. Calero, Computing the heat of adsorption using molecular simulations: the effect of strong coulombic interactions, J. Chem. Theory Comput. 4 (2008) 1107–1118.
[56] R. Krishna, J.M. van Baten, Investigating the potential of Mg-MOF74 membranes for CO2 capture, J. Membr. Sci. 377 (2011) 249–260.
[57] A.N. Dickey, A.O. Yazaydin, R.R. Willis, R.Q. Snurr, Screening CO2/N2 selectivity in metal-organic frameworks using monte carlo simulations and ideal adsorbed solution theory, Can. J. Chem. Eng. 90 (2012) 825–832.
[58] Y.G. Chung, D.A. Gómez-Gualdrón, P. Li, K.T. Leperi, P. Deria, H. Zhang, N.A. Vermuelen, J.F. Stoddart, F. You, J.T. Hupp, O.K. Farha, R.Q. Snurr, In silico discovery of metal-organic frameworks for precombustion CO2 capture using a genetic algorithm, Sci. Adv. 2 (2016) 1–9.
[59] X. Shao, Z. Feng, R. Xue, C. Ma, W. Wang, X. Peng, D. Cao, Adsorption of CO2, CH4, CO2/N2 and CO2/CH4 in novel activated carbon beads: preparation, measurements and simulation, AIChE J. 57 (2011) 3042–3051.
[60] Z. Hu, M. Khurana, Y.H. Seah, M. Zhang, Z. Guo, D. Zhao, Ionized Zr-MOFs for highly efficient post-combustion CO2 capture, Chem. Eng. Sci. 124 (2015) 61–69.
[61] S. Xiang, Y. He, Z. Zhang, H. Wu, W. Zhou, R. Krishna, B. Chen, Microporous metal-organic framework with potential for carbon dioxide capture at ambient conditions, Nat. Commun. 3 (2012) 954.
[62] A.H. Berger, A.S. Bhown, Comparing physisorption and chemisorption solid sorbents for use separating CO2 from flue gas using temperature swing adsorption, Energy Proc. 4 (2011) 562–567.
[63] D. Wiersum, J.S. Chang, C. Serre, P.L. Llewellyn, An adsorbent performance indicator as a first step evaluation of novel sorbents for gas separations: application to metal-organic frameworks, Langmuir 29 (2013) 3301–3309.
[64] M.S.A. Baksh, F. Notaro, Method for production of nitrogen using oxygen selective adsorbents, US Patent 5735938, 1998.
[65] S.U. Rege, R.T. Yang, A simple parameter for selecting an adsorbent for gas separation by pressure swing adsorption, Sep. Sci. Technol. 36 (2001) 3355–3365.
[66] Z. Liu, C.A. Grande, P. Li, J. Yu, A.E. Rodrigues, Multi-bed vacuum pressure swing adsorption for carbon dioxide capture from flue gas, Sep. Purif. Technol. 81 (2011) 307–317.
[67] R. Kumar, Pressure swing adsorption process: performance optimum and adsorbent selection, Ind. Eng. Chem. Res. 33 (1994) 1600–1605.
[68] M.T. Ho, G.W. Allinson, D.E. Wiley, Reducing the cost of CO2 capture from flue gases using pressure swing adsorption, Ind. Eng. Chem. Res. 47 (2008) 4883–4890.
[69] L. Bastin, P.S. Barcia, E.J. Hurtado, J.A.C. Silva, A.E. Rodrigues, B. Chen, A microporous metal-organic framework for separation of CO2/N2 and CO2/CH4 by fixed-bed adsorption, J. Phys. Chem. C 112 (2008) 1575–1581.
[70] P.D. Jadhav, S.S. Rayalu, R.B. Biniwale, S. Devotta, CO2 emission and its mitigation by adsorption of zeolites and activated carbon, Curr. Sci. 92 (2007) 724–726.
[71] R. Krishna, J.R. Long, Screening metal-organic frameworks by analysis of transient breakthrough of gas mixtures in a fixed bed adsorber, J. Phys. Chem. C 115 (2011) 12941–12950.
[72] Y. He, R. Krishna, B. Chen, Metal-organic frameworks with potential for energy-efficient adsorptive separation of light hydrocarbons, Energy Environ. Sci. 5 (2012) 9107–9120.
[73] H. Wu, K. Yao, Y. Zhu, B. Li, Z. Shi, R. Krishna, J. Li, Cu-TDPAT, an rht-type dual-functional metal-organic framework offering significant potential for use in H2 and natural gas purification processes operating at high pressures, J. Phys. Chem. C 116 (2012) 16609–16618.
[74] R. Krishna, R. Baur, Modelling issues in zeolite based separation processes, Sep. Purif. Technol. 33 (2003) 213–254.
[75] A.L. Myers, J.M. Prausnitz, Thermodynamics of mixed-gas adsorption, AIChE 11 (1965) 121–127.
[76] C.W. Skarstrom, Method and apparatous for fractionating gaseous mixtures by adsorption, US Patent 2944627, 1960.
[77] Y. Chung, B.K. Na, H.K. Song, Short-cut evaluation of pressure swing adsorption systems, Comput. Chem. Eng. 22 (1998) S637–S640.
[78] W.K. Choi, T.I. Kwon, Y.K. Yeo, H. Lee, B.K. Na, H.K. Song, Optimal operation of the pressure swing adsorption (PSA) process for CO2 recovery, Korean J. Chem. Eng. 20 (2003) 617–623.
[79] A.L. Chaffee, G.P. Knowles, Z. Liang, J. Zhang, P. Xiao, P.A. Webley, CO2 capture by adsorption: materials and process development, Int. J. Green. Gas Control. 1 (2007) 11–18.
[80] L. Riboldi, O. Bolland, J.M. Ngoy, N. Wagner, Full-plant analysis of a PSA CO2 capture unit integrated in coal-fired power plants: post- and pre-combustion scenarios, Energy Procedia 63 (2014) 2289–2304.
[81] D. Bahamon, L.F. Vega, Systematic evaluation of materials for post-combustion CO2 capture in a temperature swing adsorption process, Chem. Eng. J. 284 (2016) 438–447.
[82] S. Cavenati, C.A. Grande, A.E. Rodrigues, Adsorption equilibrium of methane, carbon dioxide, and nitrogen on zeolite 13X at high pressures, J. Chem. Eng. Data. 49 (2004) 1095–1101.
[83] O. Talu, Measurements and analysis of mixture adsorption equilibrium in porous solids, Chem. Ing. Technol. 83 (2011) 67–82.
[84] V.G. Gomes, K.W.K. Yee, Pressure swing adsorption for carbon dioxide sequestration from exhaust gases, Separ. Purif. Technol. 28 (2002) 161–171.
[85] L. Joos, J.M. Huck, V. Van Speybroeck, B. Smit, Cutting the cost of carbon capture: a casa for carbon capture and utilization, Faraday Discuss. 192 (2016) 391.
[86] K.T. Leperi, R.Q. Snurr, F. You, Optimization of two-stage pressure/vacuum swing adsorption with variable dehydration level for postcombustion carbon capture, Ing. Eng. Chem. Res. 55 (2016) 3338–3359.